Mon. Not. R. Astron. Soc. **399,** 264–272 (2009) doi:10.1111/j.1365-2966.2009.15258.x

Are ^{12}CO lines good indicators of the star formation rate in galaxies?

E. Bayet,[1⋆] M. Gerin,[2⋆] T. G. Phillips[3⋆] and A. Contursi[4⋆]

[1]*Department of Physics and Astronomy, University College London, Gower Street, London WC1E 6BT*
[2]*LERMA (CNRS-UMR 8112), Observatoire de Paris and Ecole Normale Supérieure, 24 rue Lhomond, F-75005 Paris, France*
[3]*California Institute of Technology, Downs Laboratory of Physics 320-47, Pasadena, CA 91125, USA*
[4]*Max Planck Institute für Extraterrestrische Physik, Postfach 1312, 85741 Garching, Germany*

Accepted 2009 June 16. Received 2009 June 16; in original form 2009 March 27

ABSTRACT

In this paper, we investigate the relevance of using the ^{12}CO-line emissions as indicators of star formation rates (SFRs). For the first time, we present this study for a relatively large number of ^{12}CO transitions (12) as well as over a large interval in redshift (from $z \sim 0$ to 6). For the nearby sources ($D \leq 10$ Mpc), we have used our previously published homogeneous sample of ^{12}CO data, mixing observational and modelled line intensities. For higher z sources ($z \geq 1$), we have collected ^{12}CO observations from various papers and completed the data set of line intensities with model predictions which we also present in this paper. Finally, for increasing the statistics, we have included recent ^{12}CO(1–0) and ^{12}CO(3–2) observations of intermediate-z sources. Linear regressions have been calculated for identifying the tightest SFR–^{12}CO-line luminosity relationships. We show that the *total* ^{12}CO, the ^{12}CO(5–4), the ^{12}CO(6–5) and the ^{12}CO(7–6) luminosities are the best indicators of SFRs (as measured by the far-infrared luminosity). Comparisons with theoretical approaches from Krumholz & Thompson and Narayanan et al. are also performed in this paper. Although in general agreement, the predictions made by these authors and the observational results we present here show small and interesting discrepancies. In particular, the slope of the linear regressions for $J_{\rm upper} \geq 4$ ^{12}CO lines is not similar between theoretical studies and observations. On the one hand, a larger high-J ^{12}CO data set of observations might help to better agree with models, increasing the statistics. On the other hand, theoretical studies extended to high-redshift sources might also reduce such discrepancies.

Key words: ISM: molecules – galaxies: ISM – galaxies: nuclei – galaxies: starburst – infrared: galaxies – submillimetre.

1 INTRODUCTION

Fifty years ago, it has been shown that the star formation rate (SFR) is intimately linked with the reservoir of the gas from which stars are forming (Schmidt 1959). The Kennicutt–Schmidt power law parametrized on local galaxies by Kennicutt (1998a,b) and Kennicutt et al. (2007) has led to an SFR index of $N = 1.4 \pm 0.15$. Since late 1990s, researchers have converted the Kennicutt–Schmidt law into a more interesting relationship connecting the SFR (traced by the infrared luminosity – hereafter $L_{\rm ir}$) to the mass of molecular gas, investigating various molecular tracers. First, Sanders, Scoville & Soifer (1991) and Sanders & Mirabel (1996) have shown that the SFR is roughly proportional to the ^{12}CO($J = 1$–0) line [hereafter CO(1–0)] luminosity (slope of 1.4–1.6, consistent with the Kennicutt–Schmidt law index). This SFR–CO(1–0) relationship has been broadly interpreted as an increase of star formation efficiency (SFE) as a function of molecular gas mass (and density). More recent analysis, focusing on tracers of *dense* molecular gas such as the HCN(1–0) line (Gao & Solomon 2004a,b; Wu et al. 2005), the HCN(3–2) line (Bussmann et al. 2008) or the CO(3–2) line (Yao et al. 2003; Narayanan et al. 2005), has shown that these transitions are likely to be better indicators of SFR than the total H_2 content [traced by the CO(1–0) luminosity]. Indeed, the CO(1–0) line can be excited at rather low densities ($\sim 10^2$–10^3 cm^{-3}) and low temperature ($\sim$5 K above ground) whereas the higher J CO transitions and the HCN lines trace denser and warmer gas, more closely connected with the stars in formation. However, recent modelling work (Krumholz & Thompson 2007; Narayanan et al. 2008) shows that this situation is more complex than it appears, involving in particular the values of the molecular line critical densities as compared with the mean gas density of the observed regions.

So far, none of the observational or modelling work investigated the relationship between the SFR and molecular gas tracers, both for *several transitions* (>2) of the same molecule (here CO) and over

⋆E-mail: eb@star.ucl.ac.uk (EB); gerin@lra.ens.fr (MG); tgp@submm.caltech.edu (TGP); contursi@mpe.mpg.de (AC)

several factors of redshift (here $z \approx 0$–6). In this paper, the influence of the high-J CO lines is especially studied. This is motivated by the fact that in addition of obtaining much more accurate estimation of the CO-line luminosities when adding the high-J transitions (see Bayet et al. 2004, 2006), more subtle effect may be revealed by these lines, when considering their respective critical densities.

The knowledge of the global star formation history, and for individual galaxies, of their actual and past SFR, is a key item for understanding galaxy evolution and for comparing with state-of-the-art models. Statistical relations linking star formation properties with other galaxy global characteristics, established by observing nearby galaxies, have already been used to understand the processes ruling the large-scale star-forming activities (e.g. Malhotra et al. 2001; Boselli, Lequeux & Gavazzi 2002). Such trends can afterwards be used in the large-scale cosmological models, which lack the spatial and temporal resolution to describe the local details of star formation in individual galaxies.

In this paper, we have thus compared the CO-line emissions (from $J = 1$–0 to 12–11 transitions) with the infrared emission for the nearby galaxies we have surveyed using the Caltech Submillimetre Observatory (CSO) (see Bayet et al. 2004, 2006). We extended this comparison to higher redshifted sources ($z = 1.4$–6.4) for which CO-line emissions have been previously observed (Cox et al. 2002; Bertoldi et al. 2003; Pety et al. 2004; Walter et al. 2004; Greve et al. 2005; Solomon & Vanden Bout 2005; Tacconi et al. 2006; Weiß et al. 2007). For these distant objects, we derived the *total* and the individual CO-line emissions (from $J = 1$–0 to 12–11) by the same approach as the one presented in Bayet et al. (2004, 2006). In order to strengthen the results with a more statistical point of view, we have finally included additional literature, CO(1–0) and CO(3–2) data from Gao & Solomon (2004a,b), Yao et al. (2003) and Narayanan et al. (2005), respectively.

The paper is divided straightforwardly as follows. Section 2 presents the data sample while Section 3 lists the results we have obtained, focusing especially on the comparison with the model predictions from Krumholz & Thompson (2007) and Narayanan et al. (2008). Finally, we conclude in Section 4.

2 SAMPLE SELECTION

It has been crucial to determine, or find in the literature, the total CO-line emission as well as the individual-line emissions of the CO transitions from $J = 1$–0 to 12–11. The total infrared luminosity (from 8 to 1000 μm) for both the nearby and the high-z sources has also been crucial to determine. Here, we have converted all the gathered data, for the first time, into a *coherent* and *homogeneous* sample we have corrected for various effects, as described below. In Table 1 and Fig. 1, the observed CO data for nearby and distant sources are presented, respectively. Model predictions go up to the $J = 15$–14 transition of CO, consistent with the work of Bayet et al. (2004, 2006). However, we have restricted our study to only the first 12 CO transitions, higher J CO lines having very weak intensity (see Bayet et al. 2004, 2006 and Fig. 1). In the rest of the paper, the *total* CO will thus refer to the sum of only the first 12 CO transitions.

2.1 Nearby sources

The CO data we are using in this study for the nearby sources are from the observational and modelling work of Bayet et al. (2004, 2006). They already provided a consistent line intensity sample for eight nearby (<10 Mpc) galaxies: NGC 253, IC 10, IC 342, NGC 6946, M83, Henize 2−10 and the Antennae (NGC 4038 and Overlap) from CO(1–0) to CO(15–14). We converted the first 12 CO integrated line intensities into luminosities (in K km s^{-1} pc^2) using the formulae in Solomon & Vanden Bout (2005):

$$L'_{\rm CO} = 3.25 \times 10^7 \times S_{\rm CO}\Delta v \times \nu_{\rm obs}^{-2} \times (1+z)^{-3} \times D_L^2, \quad (1)$$

where z is the redshift,[1] $\nu_{\rm obs}$ is the observed frequency[2] (in GHz) of the CO line, $S_{\rm CO}\ \Delta v$ is the CO integrated line intensities (in Jy km s^{-1}) and D_L is the luminosity distance (in Mpc).[3] The total CO luminosity has been obtained by summing the individual CO-line luminosities, converted previously from equation (1) into solar luminosity units ($L_\odot$) to avoid any frequency bias in the SFR–total CO relationship. Table 2 summarizes the results obtained.

Table 1. List of the detected CO lines for nearby galaxies included in this study. These CO-line detections are from Bayet et al. (2004, 2006). Similar information for distant sources is found in Fig. 1 (observations represented by black bullets). When the line is not detected, we have used its corresponding predicted emission from modelling work (see Sections 2.1 and 2.2). For the Antennae sources (NGC 4038 and Overlap), the ^{12}CO(4–3) and ^{12}CO(7–6) lines have been observed by Bayet et al. (2006) but they suffer from large uncertainties. Therefore, we used for these two objects and two transitions rather the corresponding best model predictions.

Name	Distance (Mpc)	Detected ^{12}CO lines
Nearby sources		
IC 10	1.0[1]	1–0, 2–1, 3–2, 4–3, 6–5, 7–6
NGC 253	2.5[2]	1–0, 2–1, 3–2, 4–3, 6–5, 7–6
IC 342	1.8[3]	1–0, 2–1, 3–2, 4–3, 6–5, 7–6
He 2–10	9.0[4]	1–0, 2–1, 3–2, 4–3, 6–5, 7–6
NGC 4038	13.8[5]	1–0, 2–1, 3–2, 4–3, 6–5, 7–6
Overlap[a]	13.8[5]	1–0, 2–1, 3–2, 4–3, 6–5, 7–6
M83	3.5[6]	1–0, 2–1, 3–2, 4–3, 6–5
NGC 6946	5.5[7]	1–0, 2–1, 3–2, 4–3, 6–5

[a]Overlap corresponds to a shifted position from the NGC 4039 nucleus in the Antennae Galaxy which shows a high gas density (see Bayet et al. 2006). References: [1]Massey & Armandroff (1995); [2]Adopted value from Mauersberger et al. (1996); [3]McCall (1989); [4]Kobulnicky & Johnson (1999); [5]Saviane, Hibbard & Rich (2004); [6]Thim et al. (2003) and [7]Tully (1988).

The infrared data used for the nearby sources and, more generally, in the whole paper, are from Sanders et al. (2003). For consistency with the additional literature data described in Section 2.3, we chose to use the total infrared luminosity from 8 to 1000 μm ($L_{\rm ir:8-1000\,\mu m}$), thereby including the continuum emission shorter than 60 μm affected by the contribution from very small grains. This total infrared luminosity is known to be contaminated by a possible active galactic nuclei (AGN) contribution (see also Graciá-Carpio et al. 2008). In particular, the AGN yield can be fairly large in the MIR range (e.g. Rowan-Robinson & Crawford 1989) in active galaxies such as luminous infrared galaxies (LIRGs) and ultra-luminous infrared galaxies (ULIRGs). However, for the sample of the nearby sources we are studying here, this AGN contamination is considered as negligible since none of the eight sources (IC 10, NGC 253, IC 342, Henize 2−10, NGC 4038, Overlap, M83 and NGC 6946) is known for hosting an AGN (see e.g. Wilson et al. 2000; Israel & Baas 2001;

[1] For nearby sources we used the NASA/IPAC Extragalactic Database (NED) values of z.

[2] The observed frequency is equal to the rest frequency $\nu_{\rm rest}$ divided by $(1+z)$.

[3] For all the sources, we obtained the luminosity distance using the web site calculator of http://www.astro.ucla.edu/∼wright/CosmoCalc.html, within a cosmology of $H_0 = 77$ km s^{-1} Mpc^{-1}, $\Omega_{\rm M} = 0.27$ and $\Omega_{\rm V} = 0.73$.

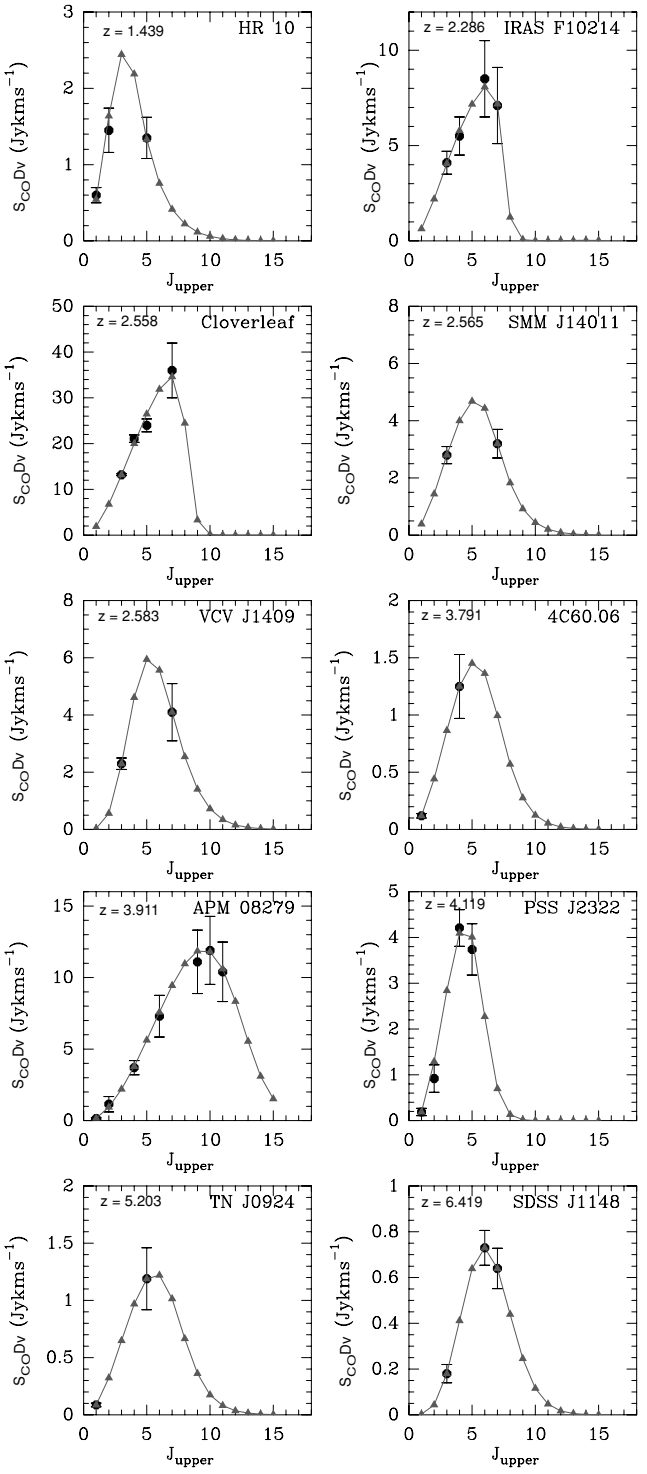

Figure 1. Observed and predicted CO spectral energy distributions (SADs) (Jy km s^{-1}) of the following high-redshift sources (from top to bottom, and by increasing order of redshift): HR 10, IRAS F10214, The Cloverleaf QSO, SMM J14011, VCV J1409, 4C60.06, APM 08279, PSS J2322, TN J0924 and SDSS J1148 (see plots). Observations and their corresponding error bars are represented by black bullets (see references listed in Solomon & Vanden Bout 2005) while LVG predictions (see Appendix A) are symbolized with grey triangles. To make the plots more easily readable, we have connected the CO LVG predictions (grey lines). One could note that, except for the source HR 10, the position of the maximum of the SED is located at rather high J ($J_{\rm upper} \geq 4$).

Kramer et al. 2005; Leroy et al. 2006; Martín et al. 2006; Usero et al. 2006, respectively).

A more important aspect of nearby sources is that the CO measurements (both observations and model predictions) referred to an aperture of 22 arcsec, as described by Bayet et al. (2004, 2006), while the infrared data from Sanders et al. (2003) showed a higher aperture (80 arcsec). Thus in Fig. 2, where we present various SFR–CO luminosity relationships (see Section 3), we compare, for nearby sources, two emitting regions which are not spatially identical. Indeed, the region which emits the infrared luminosity is larger than the region where CO is detected. It is the same case for the intermediate-z data (Section 2.3), but this problem does not appear in the case of higher z sources since they are seen as point-like sources in both the sub-mm/mm and infrared wavelengths. To correct this effect on nearby and intermediate-z sources, we have estimated a factor between the CO and the $L_{\rm ir}$ resolution via the dust emission traced by SCUBA maps at 850 μm. We have derived from these maps the luminosity (removing the background contribution) of the 850-μm emission at a spatial resolution of 22 and 80 arcsec, for the sources available in the SCUBA archive. We have then calculated the ratio between the emissions observed at 22 and 80 arcsec that we have applied to the infrared data. We have obtained ratios varying from 2.3 to 6.5, depending on the source. Rather than the 450 μm SCUBA maps, we have chosen the 850-μm SCUBA maps because they show a better signal-to-noise ratio. Nevertheless, we checked that the factors obtained at 850 μm were in agreement with the ones at 450 μm (difference obtained being less than 2 per cent). After having applied such correction to the infrared data of the galaxies in common to this paper and the SCUBA archive, we have however obtained similar results to those listed in Table 3 and presented in Fig. 2 which show non-aperture-corrected data. The slopes did not show changes greater than 5 per cent in their values, depending on the SFR–CO-line luminosity relationship studied. Due to the fact that all the data could not be corrected consistently for this effect since the galaxies presented here have not been all observed by SCUBA (e.g. IC 342), we thus have decided to keep non-corrected infrared data in Fig. 2, increasing however the error bars on the slope values by 5 per cent in Table 3.

Both the (non-aperture-corrected) infrared and the CO luminosities used in Fig. 2 are listed in Table 2.

2.2 High-z sources

So far, a complete *observed* CO SED does not exist for $J = 1$–0 to 12–11 neither for nearby nor for high-z sources.

However, at high redshift, various CO transitions have already been detected (e.g. Cox et al. 2002; Bertoldi et al. 2003; Pety et al. 2004; Walter et al. 2004; Greve et al. 2005; Solomon & Vanden Bout 2005; Tacconi et al. 2006; Weiß et al. 2007). Most of these data are summarized in Solomon & Vanden Bout (2005). In our study, we restricted the number of studied sources presented in Solomon & Vanden Bout (2005) to 10 objects : 4C60.07, APM 08279,[4] Cloverleaf QSO, SMM J14011, VCV J1409, PSSJ2322, TN J0924, SDSS J1148, IRAS F10214 and HR 10, keeping only those which show at least two CO-line detections. Indeed, to correctly constrain the models which estimate the missing line emissions [Large Velocity Gradient (LVG) models; see Appendix A] and derive relevant predicted CO-line intensities, it is crucial to have as many CO-line

[4] For this source, we rather used more recent CO data from Weiß et al. (2007).

Table 2. Infrared and CO-line luminosities of the sources in our sample (see square symbols in Fig. 2). For distant galaxies, we also list in the last column the lens magnification factor we have found in Solomon & Vanden Bout (2005) and use in this study (see Fig. 2). Intermediate-z source values are not shown in this table since they are already described in details in the references mentioned in the text. When an asterisk is seen, it means that the value has been estimated from observations only.

Name	$L_{\rm ir}{}^a$ ($L_\odot$)	$L'_{\rm CO(tot)}{}^b$ ($L_\odot$)	Ref.	$L'_{\rm CO(1-0)}$ (K km s^{-1} pc^2)	Ref.	$L'_{\rm CO(3-2)}$ (K km s^{-1} pc^2)	Ref.	$L'_{\rm CO(7-6)}$ (K km s^{-1} pc^2)	Ref.	Lens magn. factor
IC 10	8.2×10^9	4.4×10^2	1 & 2	$5.6 \times 10^{6*}$	1 & 2	$3.5 \times 10^{5*}$	1 & 2	$7.3 \times 10^{3*}$	1 & 2	
NGC 253	2.8×10^{10}	3.3×10^5	2 & 3	$1.5 \times 10^{9*}$	1 & 2	$1.4 \times 10^{8*}$	1 & 2	$8.0 \times 10^{6*}$	1 & 2	
IC 342	1.5×10^{10}	8.4×10^3	1 & 2	$1.6 \times 10^{8*}$	1 & 2	$9.7 \times 10^{6*}$	1 & 2	$1.2 \times 10^{5*}$	1 & 2	
He 2–10	6.2×10^9	3.4×10^4	2 & 3	$2.1 \times 10^{8*}$	1 & 2	$1.1 \times 10^{7*}$	1 & 2	$1.0 \times 10^{6*}$	1 & 2	
NGC 4038	6.9×10^{10}	5.5×10^5	1 & 2	$2.1 \times 10^{9*}$	1 & 2	$1.9 \times 10^{8*}$	1 & 2	$1.3 \times 10^{7*}$	1 & 2	
Overlap	6.9×10^{10}	6.7×10^5	1 & 2	$3.3 \times 10^{9*}$	1 & 2	$2.9 \times 10^{8*}$	1 & 2	$1.7 \times 10^{7*}$	1 & 2	
M83	1.3×10^{10}	1.0×10^5	1 & 2	$3.1 \times 10^{8*}$	1 & 2	$3.3 \times 10^{7*}$	1 & 2	2.7×10^6	1 & 2	
NGC 6946	1.5×10^{10}	1.0×10^5	1 & 2	$1.4 \times 10^{9*}$	1 & 2	$1.1 \times 10^{8*}$	1 & 2	1.3×10^6	1 & 2	
HR10	6.5×10^{12}	4.2×10^8	2	$5.6 \times 10^{10*}$	4 & 2	2.5×10^{10}	2	7.9×10^8	2	1
IRAS F10214	3.6×10^{12}	6.6×10^9	2	1.4×10^{11}	2	$9.9 \times 10^{10*}$	4 & 2	$3.2 \times 10^{10*}$	4 & 2	17
Cloverleaf	5.4×10^{12}	4.3×10^{10}	2	5.0×10^{11}	2	$3.9 \times 10^{11*}$	4 & 2	$1.9 \times 10^{11*}$	4 & 2	11
SMM J14011	2.4×10^{12}	6.1×10^9	2	1.0×10^{11}	2	$8.3 \times 10^{10*}$	4 & 2	$1.7 \times 10^{10*}$	4 & 2	8.3
VCV J1409	3.5×10^{13}	7.8×10^9	2	9.6×10^9	2	6.9×10^{10}	4 & 2	2.3×10^{10}	4 & 2	1
4CO60.07	1.3×10^{13}	4.8×10^9	2	$6.1 \times 10^{10*}$	4 & 2	4.9×10^{10}	2	1.0×10^{10}	2	1
APM 08279	2.9×10^{13}	1.1×10^{11}	2	$8.0 \times 10^{10*}$	5 & 2	1.3×10^{11}	5 & 2	1.0×10^{11}	5 & 2	7
PSS J2322	9.3×10^{12}	9.6×10^9	2	$1.1 \times 10^{11*}$	4 & 2	1.8×10^{11}	2	8.3×10^9	2	2.5
TN J0924	7.0×10^{12}	9.9×10^9	2	$7.3 \times 10^{10*}$	4 & 2	6.0×10^{10}	2	1.7×10^{10}	2	1
SDSS J1148	2.7×10^{13}	9.1×10^9	2	3.5×10^9	2	2.2×10^{10}	4 & 2	1.5×10^{10}	4 & 2	1

$^a L_{\rm ir}$ is the 8–1000 μm total infrared luminosity deduced from either Sanders et al. (2003) (nearby sources) or Solomon & Vanden Bout (2005) (high-z galaxies). For the distant objects, $L_{\rm ir}$ are corrected from the lens magnification effect (see text in Section 2.2).

$^b L'_{\rm CO(tot)}$ is the total CO-line luminosity obtained after the use of models for predicting the emission of the missing (non-observed) CO lines (see Sections 2.1 and 2.2 and, for more details, the Appendix A and the modelling work of Bayet et al. 2004; Bayet et al. 2006). References: [1]See Bayet et al. (2006); [2]this work; [3]Bayet et al. (2004); [4]Solomon & Vanden Bout (2005) and [5]Weiß et al. (2007).

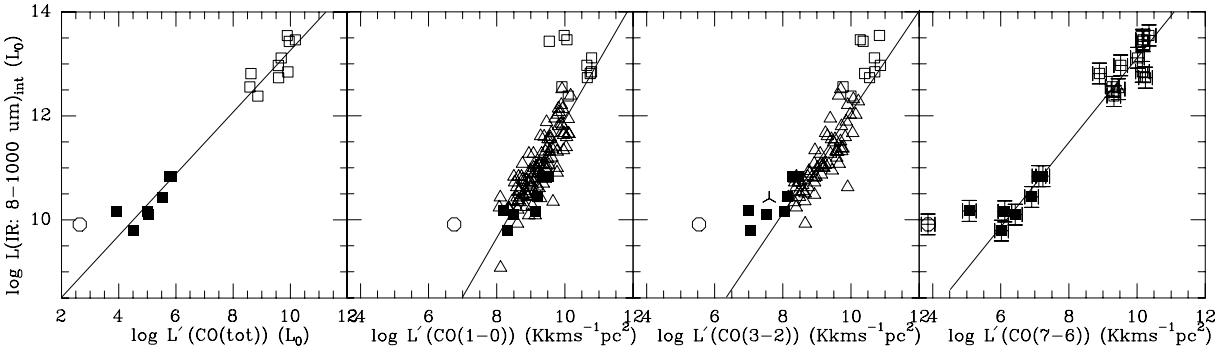

Figure 2. Examples of SFR–CO-line luminosity relationships we have obtained, expressed in log–log scales. From left to right, we plotted the total integrated infrared luminosity $L_{\rm ir:8-1000\mu m}$ (in $L_\odot$) versus the total CO (in $L_\odot$), the CO(1–0), the CO(3–2) and the CO(7–6) luminosities (in K km s^{-1} pc^2) (see Section 2). The squares correspond to the sources we studied in details in this paper (see Sections 2.1 and 2.2) while the triangles correspond to the literature data we have added from Yao et al. (2003), Gao & Solomon (2004a,b), Narayanan et al. (2005) (see Section 2.3). The black filled squares represent the nearby sources while the white opened squares symbolize the high-z sources. In all plots, IC 10 is separated from other nearby sources (see Section 3.1) and represented by open white circles. In the plot representing the SFR–CO(3–2) luminosity relationship, one can see a lambda symbol corresponding to the source NGC 7817 we have also excluded (see Section 3.1). The linear regressions have been obtained using the XMGRACE software. They are represented by black lines. For keeping the figures clear, we plotted the typical error bars of the observations (included in the calculations of the linear regressions), only on the SFR–CO(7–6) luminosity correlation. These errors correspond to $\pm 1\sigma$ uncertainties both on the $L_{\rm ir}$ and on the molecular CO-line luminosities.

detections as possible. This is why we have rejected from our study high-z sources presented in Solomon & Vanden Bout (2005) with only one CO line observed.

To estimate the *total* CO luminosity as well as the individual missing molecular CO-line luminosities in these sources, we have used a single-component LVG model as done in Bayet et al. (2004, 2006). The obtained line intensity predictions (see Fig. 1) correspond to a beam size of 22 arcsec, consistently with other data sets. The goal of the paper is to investigate the SFR–molecular CO-line luminosity relationships. Thus, we will not discuss further the physical properties of the molecular gas we have obtained using the LVG model. None the less, we present them in Appendix A.

In Fig. 1, we have superimposed on the CO observations (black bullets with error bars), the predicted emissions of both the

Table 3. Results of the linear regressions (slope and correlation coefficients) for the relationships between SFR and the CO transitions from $J = 1$–0 to 12–11 (see Fig. 2 for some examples of SFR–CO-line correlations). The linear regressions have been obtained using the software XMGRACE, including the error bars of the observations in the calculations. In these linear regressions, we excluded two sources from the calculations: IC 10 for all the regressions and NGC 7817 for the SFR–CO(3–2) relationship (see Section 3.1). We have isolated the SFR–total CO luminosity relationship from others because we have used different units.

Molecular line luminosities	Slope	Correlation coeff.	Number of sources
CO(1–0)[a]	1.41 ± 0.26	0.82	17
CO(1–0)[b]	1.14 ± 0.08	0.82	103
CO(2–1)	1.20 ± 0.10	0.95	17
CO(3–2)[a]	1.00 ± 0.07	0.97	17
CO(3–2)[b]	0.99 ± 0.06	0.89	81
CO(4–3)	0.94 ± 0.05	0.98	17
CO(5–4)	0.90 ± 0.04	0.98	17
CO(6–5)	0.86 ± 0.04	0.98	17
CO(7–6)	0.80 ± 0.04	0.98	17
CO(8–7)	0.74 ± 0.05	0.97	17
CO(9–8)	0.67 ± 0.06	0.94	17
CO(10–9)	0.61 ± 0.07	0.92	17
CO(11–10)	0.57 ± 0.07	0.90	17
CO(12–11)	0.53 ± 0.07	0.89	17
CO(tot)	0.62 ± 0.04	0.97	16[c]

[a]Without any additional literature data.
[b]With additional literature data.
[c]Markarian 231 is not included in this linear regression calculation because we did not find any estimation of its CO(11–10) and CO(12–11) line- luminosities needed for estimating properly its total CO luminosity.

observed and the missing CO lines (grey filled triangles). Similar to the nearby sources case, the total CO luminosity has been obtained by summing the individual CO-line luminosities converted previously from equation (1) into solar luminosity units ($L_\odot$) to avoid any frequency bias in the SFR–total CO relationship. More precisely, we have used the observed velocity-integrated CO-line fluxes ($S_{CO}\Delta v$ in Jy km s^{-1}) when detected and the predicted values when not. The redshift values used in equation (1) are those presented in Solomon & Vanden Bout (2005).

We did not need to correct the CO-line luminosities for any beam dilution effect since the high-z galaxies are point-like sources within telescope beams and show unresolved emissions whatever these wavelengths. However, some of these distant objects are lensed. Thus, we have applied the factor of lens magnification listed in Solomon & Vanden Bout (2005) to *all* the CO-line luminosities. The underlying assumption of such a correction is that the gravitational lens magnifies similarly the emission from compact and warm regions usually traced by high-J CO lines such as the CO(7–6) line and the regions more extended normally traced by typical low-J lines such as the CO(1–0) transition. In principle, this is a relevant assumption since the properties of the lens do not depend on the magnified source but only on the properties of the galaxies separated the observer from the studied source.

For the infrared luminosity, we used the integrated values ['L_{FIR}(int.)'] listed in table 1 of Solomon & Vanden Bout (2005), corresponding to infrared emission corrected for lens magnification. After having checked several references in this table, it appears that the 'L_{FIR}(int.)' values are similar to the $L_{ir:8-1000\,\mu m}$ presented in Sanders et al. (2003) (see the example of HR 10 for which Dey et al. 1999 derived the infrared luminosity by fitting the dust SED on a rest wavelength range from 10 μm to 2 cm).

For these distant sources, we also present in Table 2 both the infrared and the CO luminosities we have used in Fig. 2.

2.3 Intermediate-z data from the literature

We have included in our study CO data from observations at intermediate redshift (within similar beam sizes) to better constrain the SFR–molecular CO-line luminosity relationships, and especially increase the statistics. These data are either from Gao & Solomon (2004a,b) [CO(1–0) transition observed with a 22 arcsec beam size], or from Yao et al. (2003) and Narayanan et al. (2005) [CO(3–2] line observed with a 15 and 22 arcsec beam sizes, respectively). We have not included the CO(2–1) data reported in Rigopoulou et al. (1996) (beam size of 23 arcsec) because they appear inconsistent with those presented in Yao et al. (2003), Gao & Solomon (2004a,b),and Narayanan et al. (2005). We have included in our SFR–CO relationships the observed and modelling results dedicated to Markarian 231 (Papadopoulos, Isaak & van der Werf 2007), providing CO-line luminosities estimations up to the CO(10–9). For the infrared luminosity values, we have used the values reported in Sanders et al. (2003) and not those listed in each corresponding papers.

The additional sources included here are seen to be mostly LIRGs and ULIRGs (at a distance $>$ 10 Mpc). Radio continuum maps (Condon et al. 1990), and the H I and SCUBA 850-μm maps (Thompson et al. 2002), show that much of the emission of the objects is extended with respect to the beam size of 15 arcsec. However, in recent high-resolution (2–3 arcsec) millimetre wave observations of seven LIRGs/ULIRGs, Bryant & Scoville (1999) find that nearly all of the detected CO($J = 1$–0) emission is concentrated within the central 1.6 kpc in six of seven objects. Because it is unlikely that there will be significant high-J CO emission where there is no CO(1–0) detected, we assume that all of the emitting gas in these additional sources is confined within the same region. Consequently, we have not converted the 14 arcsec beam data into that for a 22-arcsec beam.

As for nearby galaxies, the infrared luminosities of these sources are expressed for a larger aperture than the one used for the CO data. As previously mentioned (see Section 2.1), this effect on the SFR–CO-line luminosity relationship has been investigated through SCUBA data. Unfortunately, as for the case of nearby galaxies, the intermediate-z sources we are using here have indeed not been *all* observed by SCUBA, therefore no correction on their infrared data has been performed directly. We have, however, taken fully into account the effect of different spatial resolutions on the slope values listed in Table 3 (increased error bars as explained in Section 2.1).

In the samples presented in Yao et al. (2003), Gao & Solomon (2004a,b) and Narayanan et al. (2005), some sources such as ARP 220 are common. For removing any calibration effects on the SFR–CO relationships, we have followed the recommendation of Narayanan et al. (2005) and applied their scaling factor equal to 0.26 for the CO(3–2) and to 0.45 for the CO(1–0). They specified that this effect may indeed occur when various instruments (and thus various calibration processes) are used.

Note that the intermediate-z sources significantly increase the number of CO observations used in the correlations either in the SFR–CO(1–0) line luminosity or in the SFR–CO(3–2) line luminosity relationships (see triangles in Fig. 2 as well as the fourth column in Table 3). This strengthens the corresponding results.

3 RESULTS

3.1 General arguments

We present in Fig. 2 the SFR–CO-line luminosity relationships we have obtained for the total CO-line emission, the CO(1–0), CO(3–2) and CO(7–6) line emissions. In the same vein, we have obtained the SFR–CO-line luminosity relationships for the other CO transitions: $J = 2$–1 and from $J = 4$–3 to 12–11. SFR–CO luminosity relationships for CO data higher than CO(7–6) are less relevant than the correlation involving lower J CO lines. Indeed, most of the data in CO(8–7), CO(9–8), CO(10–9), CO(11–10) and CO(12–11) are from modelled fit, similarly to the fits presented in Fig. 1. In such cases, correlations between the SFR and the CO luminosity are not constrained by many observational measures. Thus, we exclude these correlations from the following analysis.

As one can see in Fig. 2, a proportionality exists between the CO and infrared luminosities over a large range of redshift (galaxies from $z \sim 0$ to 6 sources). This characteristic has been previously seen (Sanders et al. 1991; Sanders & Mirabel 1996 and references therein), although this sample was more restricted in redshift than the one we present in this paper. It has been interpreted as an increasing SFE [SFR divided by M(H_2)] as a function of molecular gas mass. Here, our data sample confirms this broad interpretation.

To quantify better these relationships, we performed linear regressions (using the software XMGRACE). The corresponding output parameters are listed in Table 3. Note that IC 10 has been excluded from these calculations. For the SFR–CO(3–2) relationship we have also excluded NGC 7817, as Narayanan et al. (2005) suggested. Indeed these two sources show very small $L'_{\rm CO}$ value with respect to the locus of other objects. This is especially true for IC 10 over several CO transitions (see Fig. 2).

Deviations from the SFR–CO trend can be expected for subsolar metallicity such as IC 10 [12 log(O/H) = 8.31 ± 0.2 from Arimoto, Sofue & Tsujimoto 1996]. As shown by Lequeux et al. (1994), a CO deficit (and a [C II] excess), relative to the infrared luminosity is expected for low metallicity systems. At low metallicity, molecular hydrogen can still be formed on grains, although the threshold between atomic and molecular hydrogen is slightly shifted compared to what is seen in our Galaxy (see the discussion on the FUSE results by Tumlinson et al. 2002). In addition, CO is more easily destroyed by FUV photons than H_2. In diffuse and translucent clouds, the decrease of CO photodissociation with increasing A_v is provided by the combined effect of self-shielding and dust extinction. At lower metallicities, these two effects get weaker, hence CO can not survive at small A_v. In molecular clouds, CO survives in the core, but an extended envelope where carbon is ionized is also present. Therefore, the CO emission is decreased, (and the [C II] emission increased) relative to normal metallicity conditions.

Over the last years, in the literature, other tracers of molecular gas have been investigated as SFR indicators, such as the HCN (Gao & Solomon 2004a,b; Vanden Bout, Solomon & Maddalena 2004; Carilli et al. 2005; Bussmann et al. 2008). The linear and tighter relationship shown between the HCN(1–0) line luminosity and the infrared luminosity, as compared to the relation SFR–CO(1–0), has been first interpreted by the fact that the HCN is a molecule tracing warmer and denser gas, more closely link with the stars in formation. Indeed, the CO(1–0) tends to emit from both dense core and more diffuse molecular filaments and cloud atmosphere ($n_{\rm crit} \sim 10^2$–10^3 cm^{-3}), leading to a non-linear relationship, whereas the HCN is typically only thermalized in the dense cores of molecular clouds ($n_{\rm crit} \sim 10^5$ cm^{-3}), thus allowing linearity. However, the fact that, in a similar sample of galaxies Yao et al. (2003) and Narayanan et al. (2005) also found a linear SFR–CO(3–2) relationship provide evidence against the sole HCN-related chemistry explanation [The critical density of the CO(3–2) is $n_{\rm crit} \sim 10^4$ cm^{-3}].

More recent theoretical analyses (Krumholz & Thompson 2007; Narayanan et al. 2008) have shown that the relationship between the SFR and molecular line luminosity in star-forming clouds (and thus the value of the slope of the linear regressions) depends rather on how the critical density of the molecular transition compares to the mean density of the observed sources. Lines with critical densities smaller than the mean density in a observed region [e.g. CO(1–0)] probe the total molecular gas and the SFR–molecular line relationship slope is in agreement with the Kennicutt–Schmidt index (slope ∼1.5). On the contrary, lines with critical densities larger than the mean density [e.g. HCN(1–0) and CO(3–2)] show luminosities rising faster than linearly with increasing mean gas density and the SFR–molecular line relationship is sublinear (slope < 1.0). In this paper, we *confirm observationally these conclusions* (see Table 3) extending them, in addition, to a larger interval in redshift.

3.2 More detailed analysis

Fig. 2 and Table 3 show that the SFR–CO(5–4), SFR–CO(6–5) and SFR–CO(7–6) line luminosity relationships are the tightest correlations (highest values of the correlation coefficients). Thus, between all the CO transitions, for the data sample we present here, these transitions might be considered as the *best SFR indicators in galaxies*. The total CO luminosity is also a very good tracer of SFR in galaxies since it shows a tight correlation (correlation coefficient of 0.984).

These tight SFR–high-J CO correlations contrast with the one seen for the CO(1–0) line. Indeed, even if we restrict the sample of CO(1–0) observations to only the 17 sources we used in the SFR–higher J CO-line luminosity relationships, considering like that the same statistics, the correlation coefficient of the CO(1–0) line is still the lowest (see Table 3). This has been previously mentioned by Riechers et al. (2006). In the same vein, it has been shown by Bussmann et al. (2008) that the higher J HCN line such as the HCN(3–2) transition is more tightly correlated to the SFR traced by the infrared luminosity than the HCN(1–0) line. We could thus conclude that *the CO(1–0) line is not a good indicator of* SFR *in galaxies*.

In a more detailed analysis of the plots seen in Fig. 2, it is interesting to note that, even if the linear regressions fit rather well in all cases the observations, they however become slightly not so relevant at low CO luminosity, and thus, especially, for the SFR–high-J CO relationships. This tendency is even more obvious in the SFR–CO(3–2) plot. The galaxies IC 342 and Henize 2-10 seem to be mainly responsible of this divergence. In the SFR–CO(7–6) plot as well as in the correlations involving higher J CO lines, it is more difficult to see this trend, probably because the statistics is reduced to 17 sources. This leads to a less accurate linear regression than in the SFR–CO(3–2) case. In the SFR–CO(7–6) line luminosity relationship, one could also notice that the deficit of CO luminosity of the galaxy IC 342 is even more enhanced. The fact that IC 342 is a less active galaxy and that Henize 2−10 is small in our nearby source sample may also play a role. Indeed, as compared to more active galaxies (such as NGC 253), they may contain less dense

gas. This has been recently confirmed by Bayet et al. (in preparation) who detected the CS(7–6) line with much more difficulties in IC 342 than NGC 253 (signal-to-noise ratio lower by a factor of 3 between the two sources). Consequently, more observations of high-*J* CO lines in quite nearby galaxies are needed to explain this characteristic better. Another possible explanation may also be the degree of thermalization varying from one environment to another as explained in Narayanan et al. (2008).

In the same way, it is noticeable that a small discrepancy between the linear regressions and the observations appears for sources showing the highest infrared luminosities (see Fig. 2 in the upper right-hand corners). However, contrarily to the previous case (nearby sources), this effect is not seen for the SFR–CO(7–6) plot nor for the other SFR–higher *J* CO correlations. On the contrary, it appears clearer for lower *J* CO lines. One very simple first assumption should be that this discrepancy may be caused by the fact that such active (high-*z*) galaxies is expected to have a higher per cent of dense gas than in local galaxies. Indeed these objects are known to undergo more violent star burst phases. The gas component traced by the CO(1–0) line may not be (relatively) as abundant and as bright as in the local Universe. This hypothesis may be confirmed by the localization of the CO SED maximum seen rather at high-*J* CO lines (see Fig. 1) which are known to trace warmer and denser gas (see Bayet et al. 2004, 2006).

3.3 Comparison with model predictions

It is essential to confront the results we have obtained to the model developed by Krumholz & Thompson (2007) and Narayanan et al. (2008). More especially, Narayanan et al. (2008) provided some estimations of linear regression slopes for various SFR–CO-line luminosity relationships. In Fig. 3, we have reproduced the fig. 7 of Narayanan et al. (2008) adding the new observational constraints we have obtained (see the open white circles with error bars in Fig. 3). Fig. 3 thus provides the variation of the slope of the SFR–CO luminosity relationship with respect to the transition of CO investigated.

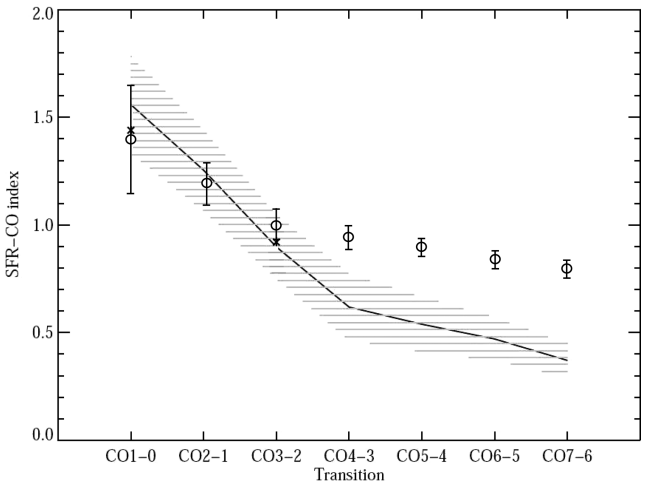

Figure 3. Predicted slopes in $\log(L_{\rm ir}) - \log(L'_{\rm CO})$ space as a function of *J* transitions of CO, as seen in the study of Narayanan et al. (2008) (fig. 7). The grey horizontal lines are the model predictions and the crosses, some observations Narayanan et al. (2008) used. Observational constraints on the slope measured from CO(1–0) to CO(7–6) presented in this paper are symbolized by open white circles (with error bars). From the CO(4–3) line, the best-fitting slopes (dashed line) given by the predictions from Narayanan et al. (2008) become not consistent with our observational results.

The best predicted (from models) SFR–CO slopes are represented by a dashed black line while the horizontal grey lines symbolize its scatter. This scatter is computed by randomly drawing a sample of 19 galaxies (which is similar to the size of our nearby and high-*z* source sample) out of a set of 100 model galaxies 1000 times. Here, our measurements are consistent with other measurements (see the crosses in Fig. 3) and with model predictions up to the SFR–CO(3–2) relationship. However, for higher *J* CO line, some discrepancies are seen. As mentioned in Narayanan et al. (2008), these discrepancies may likely due to the fact that these models do not include any high-*z* sources. Most of these sources have an increasing fraction of AGN as compared with this of the local galaxies. These embedded AGN might thus significantly contaminate the infrared luminosity of the sources (Tran et al. 2001; Kim, Veilleux & Sanders 2002; Veilleux, Kim & Sanders 2002), as well as be responsible of an increase of the gas temperature, leading to a higher slope in the linear regression. In a simple view, the star formation being warmer in such distant objects, the temperature effect is expected to be especially enhanced for the high-*J* CO line relationships. Temperature contamination, imperfectly taken into account in the models, is thus more expected in such CO lines than in low-*J* CO transitions.

4 CONCLUSIONS

In this paper we have investigated the relevance of using the CO-line emissions as indicators of SFR. For the first time, we have both studied this question over a large number of CO transitions (12) and over a large sample of source going up to a redshift of $z > 6$. We have shown that the SFR–total CO, SFR–CO(5–4), SFR–CO(6–5) and SFR–CO(7–6) line luminosity relationships are the tightest correlations, making these lines the best indicators of the SFR. The results we have obtained also strongly confirmed the predictions from Krumholz & Thompson (2007) and Narayanan et al. (2008) who showed that the SFR–CO-lines luminosity relationships are above all regulated by the Kennicutt–Schmidt law, which sets the way in which observed transitions trace molecular gas. In other words, the SFR–CO-line luminosity relationships depends on how the critical density of the molecule compares to the mean density of observed source. We confirm in this paper that, for the CO lines with $J_{\rm upper} > 3$, the SFR–CO-line luminosity relationship are indeed sublinear. However some discrepancies between model predictions and observations appear for higher *J* CO-lines [from CO(4–3)] relationships. These differences may be likely due to the fact that, in the model the high-*z* sources are not included (possible temperature contamination from AGN heating processes). Anyway, more observations (ALMA, Herschel) of CO in both nearby and high-*z* sources, especially the high-frequency CO transitions could also be very helpful for explaining these discrepancies.

ACKNOWLEDGMENTS

EB acknowledges financial support from the Leverhulme Trust. Fig. 7 of Narayanan et al. (2008; p. 1005) has been reproduced by permission of the AAS.

REFERENCES

Arimoto N., Sofue Y., Tsujimoto T., 1996, PASJ, 48, 275
Bayet E., Gerin M., Phillips T. G., Contursi A., 2004, A&A, 427, 45
Bayet E., Gerin M., Phillips T. G., Contursi A., 2006, A&A, 460, 467

Bayet E., Lintott C., Viti S., Martín-Pintado J., Martín S., Williams D. A., Rawlings J. M. C., 2008, ApJ, 685, L35
Bertoldi F. et al., 2003, A&A, 409, L47
Boselli A., Lequeux J., Gavazzi G., 2002, A&A, 384, 33
Bryant P. M., Scoville N. Z., 1999, AJ, 117, 2632
Bussmann R. S. et al., 2008, ApJ, 681, L73
Carilli C. L. et al., 2005, ApJ, 618, 586
Condon J. J., Helou G., Sanders D. B., Soifer B. T., 1990, ApJS, 73, 359
Cox P. et al., 2002, A&A, 387, 406
de Jong T., Dalgarno A., Chu S.-I., 1975, ApJ, 199, 69
Dey A., Graham J. R., Ivison R. J., Smail I., Wright G. S., Liu M. C., 1999, ApJ, 519, 610
Gao Y., Solomon P. M., 2004a, ApJS, 152, 63
Gao Y., Solomon P. M., 2004b, ApJ, 606, 271
Goldreich P., Kwan J., 1974, ApJ, 189, 441
Graciá-Carpio J., García-Burillo S., Planesas P., Fuente A., Usero A., 2008, A&A, 479, 703
Greve T. R. et al., 2005, MNRAS, 359, 1165
Israel F. P., Baas F., 2001, A&A, 371, 433
Kennicutt R. C. Jr, 1998a, ARA&A, 36, 189
Kennicutt R. C. Jr, 1998b, ApJ, 498, 541
Kennicutt R. C. Jr, 2007, ApJ, 671, 333
Kim D.-C., Veilleux S., Sanders D. B., 2002, ApJS, 143, 277
Kobulnicky H. A., Johnson K. E., 1999, ApJ, 527, 154
Kramer C., Mookerjea B., Bayet E., Garcia-Burillo S., Gerin M., Israel F. P., Stutzki J., Wouterloot J. G. A., 2005, A&A, 441, 961
Krumholz M. R., Thompson T. A., 2007, ApJ, 669, 289
Lequeux J., Le Bourlot J., Des Forets G. P., Roueff E., Boulanger F., Rubio M., 1994, A&A, 292, 371
Leroy A., Bolatto A., Walter F., Blitz L., 2006, ApJ, 643, 825
McCall M. L., 1989, AJ, 97, 1341
Malhotra S. et al., 2001, ApJ, 561, 766
Martín S., Mauersberger R., Martín-Pintado J., Henkel C., García-Burillo S., 2006, ApJS, 164, 450
Massey P., Armandroff T. E., 1995, AJ, 109, 2470
Mauersberger R., Henkel C., Wielebinski R., Wiklind T., Reuter H.-P., 1996, A&A, 305, 421
Narayanan D., Groppi C. E., Kulesa C. A., Walker C. K., 2005, ApJ, 630, 269
Narayanan D., Cox T. J., Shirley Y., Davé R., Hernquist L., Walker C. K., 2008, ApJ, 684, 996
Papadopoulos P. P., Isaak K. G., van der Werf P. P., 2007, ApJ, 668, 815
Pety J., Beelen A., Cox P., Downes D., Omont A., Bertoldi F., Carilli C. L., 2004, A&A, 428, L21
Riechers D. A. et al., 2006, ApJ, 650, 604
Rigopoulou D., Lawrence A., White G. J., Rowan-Robinson M., Church S. E., 1996, A&A, 305, 747
Rowan-Robinson M., Crawford J., 1989, MNRAS, 238, 523
Sanders D. B., Mirabel I. F., 1996, ARA&A, 34, 749
Sanders D. B., Scoville N. Z., Soifer B. T., 1991, ApJ, 370, 158
Sanders D. B., Mazzarella J. M., Kim D.-C., Surace J. A., Soifer B. T., 2003, AJ, 126, 1607
Saviane I., Hibbard J. E., Rich R. M., 2004, AJ, 127, 660
Schmidt M., 1959, ApJ, 129, 243
Solomon P. M., Vanden Bout P. A., 2005, ARA&A, 43, 677
Tacconi L. J. et al., 2006, ApJ, 640, 228
Thim F., Tammann G. A., Saha A., Dolphin A., Sandage A., Tolstoy E., Labhardt L., 2003, ApJ, 590, 256
Thompson M., Hatchell J., MacDonald G., Millar T., 2002, in Crowther P., ed., ASP Conf. Ser. Vol. 267, Hot Star Workshop III: The Earliest Phases of Massive Star Birth. Astron. Soc. Pac., San Francisco, p. 429
Tran Q. D. et al., 2001, ApJ, 552, 527
Tully R. B., 1988, Sci, 242, 310
Tumlinson J. et al., 2002, ApJ, 566, 857
Usero A., García-Burillo S., Martín-Pintado J., Fuente A., Neri R., 2006, A&A, 448, 457
Vanden Bout P. A., Solomon P. M., Maddalena R. J., 2004, ApJ, 614, L97
Veilleux S., Kim D.-C., Sanders D. B., 2002, ApJS, 143, 315
Walter F., Carilli C., Bertoldi F., Menten K., Cox P., Lo K. Y., Fan X., Strauss M. A., 2004, ApJ, 615, L17
Weiß A., Downes D., Neri R., Walter F., Henkel C., Wilner D. J., Wagg J., Wiklind T., 2007, A&A, 467, 955
Wilson C. D., Scoville N., Madden S. C., Charmandaris V., 2000, ApJ, 542, 120
Wu J., Evans N. J., II, Gao Y., Solomon P. M., Shirley Y. L., Vanden Bout P. A., 2005, ApJ, 635, L173
Yao L., Seaquist E. R., Kuno N., Dunne L., 2003, ApJ, 588, 771

APPENDIX A: SINGLE COMPONENT LVG MODELLING RESULTS FOR THE HIGH-z SOURCES

As mentioned in Section 2.2, a complete *observed* CO SED does not exist from $J = 1$–0 to 12–11 in high-z sources. We thus have collected CO-line emissions from Solomon & Vanden Bout (2005) and performed a LVG analysis to derive the missing CO integrated line intensities. The results of this modelling work are shown in Fig. 1 and in the following Table A1.

We have run LVG models (Goldreich & Kwan 1974; de Jong, Dalgarno & Chu 1975), already well described in various papers. The version we have used in this study is the one presented in Bayet et al. (2004, 2006, 2008). This LVG model is basically running with three free parameters: the gas density $n(H_2)$, the kinetic temperature (T_K) and the CO column density divided by the linewidth [$N(^{12}CO)/\Delta v$]. We have investigated the following range of LVG input parameters: $5 < T_K < 255\,K$, $1 \times 10^{12}\,cm^{-2}/km\,s^{-1} < N(^{12}CO)/\Delta v < 1 \times 10^{19}\,cm^{-2}$ and $1 \times 10^{1}\,cm^{-3} < n(H_2) < 1 \times 10^{7}\,cm^{-3}$.

For determining the missing CO-line intensities, we have constrained the predicted CO-line intensity ratios with the observed values (computed from Solomon & Vanden Bout 2005) via a reduced χ^2 method as performed in Bayet et al. (2004, 2006, 2008).

We have used a single LVG component for reproducing the entire set of CO data in high-z sources, being fully conscious that this modelling approach is not ideal for reproducing the widespread view that the ISM contains dense, star-forming molecular cloud cores and more diffuse gas in cloud envelopes, even in high-z sources. Motivated also by, on average, the small number of CO detections, we have thus considered this approach as reasonable for the purpose of this paper.

We recommend to use the predicted physical properties derived and listed in Table A1 as only indicative values. We indeed remind the reader that we were not trying to model each source individually,

Table A1. Results of the single component LVG model analysis. We presented in this table the physical properties of the best LVG model (having the lowest χ^2 value when compared to the observations).

Source	T_K (K)	$n(H_2)$ (cm^{-3})	$N(CO)/\Delta v$ ($cm^{-2}/km\,s^{-1}$)
HR10	255	1.0×10^{1}	8.0×10^{18}
IRAS F10214	15	8.0×10^{5}	3.0×10^{18}
Cloverleaf	20	4.0×10^{4}	1.0×10^{19}
SMM J14011	205	2.7×10^{1}	7.9×10^{18}
VCV J1409	185	1.7×10^{4}	4.5×10^{15}
4CO60.07	180	1.7×10^{2}	1.5×10^{18}
APM 08279	255	9.0×10^{3}	8.5×10^{17}
PSS J2322	30	5.0×10^{4}	2.2×10^{16}
TN J0924	205	1.4×10^{2}	2.5×10^{18}
SDSS J1148	100	7.9×10^{4}	4.5×10^{15}

deriving the accurate set of physical properties for the molecular gas, but that we rather aim to obtain satisfactory estimations of the CO-line intensities in these sources. Note that for APM 08279 (Weiß et al. 2007), the use of two LVG components has been made but, such as the sum of *both* CO components agrees with the observed CO SED. Thus, the choice of one or two LVG components model does not significantly affect the SFR–*total* CO luminosity relationships we present in this paper.

This paper has been typeset from a TEX/LATEX file prepared by the author.